BIOCHEMISTRY
including biophysical chemistry & molecular biology

Article

pubs.acs.org/biochemistry

Effect of β,γ-CHF- and β,γ-CHCl-dGTP Halogen Atom Stereochemistry on the Transition State of DNA Polymerase β

Keriann Oertell,[†] Yue Wu,[†] Valeria M. Zakharova,[†] Boris A. Kashemirov,[†] David D. Shock,[‡] William A. Beard,[‡] Samuel H. Wilson,[‡] Charles E. McKenna,[†] and Myron F. Goodman*[,†,§]

[†]Department of Chemistry, University of Southern California, Los Angeles, California 90089, United States

[‡]Laboratory of Structural Biology, National Institute of Environmental Health Sciences, National Institutes of Health, Research Triangle Park, North Carolina 27709, United States

[§]Department of Biological Sciences, University of Southern California, Los Angeles, California 90089, United States

Supporting Information

ABSTRACT: Recently, we synthesized the first individual β,γ-CHX-dGTP diastereomers [(*R*)- or (*S*)-CHX, where X is F or Cl] and determined their structures in ternary complexes with DNA polymerase β (pol β). We now report stereospecificity by pol β on the mixed β,γ-CHX diastereomer pairs using nuclear magnetic resonance and on the separate diastereomers using transient kinetics. For both the F and Cl diastereomers, the *R* isomer is favored over the *S* isomer for G·C correct incorporation, with stereospecificities $[(k_{pol}/K_d)_R/(k_{pol}/K_d)_S]$ of 3.8 and 6.3, respectively, and also for G·T misincorporation, with stereospecificities of 11 and 7.8, respectively. Stereopreference for the (*R*)-CHF-dGTP diastereomer was abolished for k_{pol} but not K_d with mutant pol β (R183A). These compounds constitute a new class of stereochemical probes for active site interactions involving halogen atoms. As Arg183 is unique in family X pols, the design of CXY deoxyribonucleotide analogues to enhance interaction is a possible strategy for inhibiting BER selectively in cancer cells.

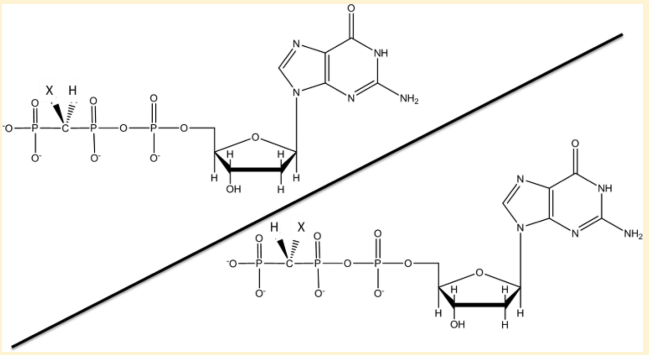

DNA polymerase β (pol β) is essential for single-nucleotide base excision repair (BER), the predominant BER pathway in humans.[1,2] This small (39 kDa) polymerase has an intrinsic lyase activity but lacks a proofreading 3′-exonuclease. Excessive levels of pol β are found in a variety of cancers,[3] and variants of pol β have been identified in as many as 30% of malignant tumors.[4−12] X-ray crystallographic studies of ternary dNTP−DNA−pol β complexes have revealed the presence of an arginine residue (Arg183) in the proximity of the triphosphate β,γ-bridging oxygen of dNTPs bound in the active site of the enzyme. This residue has no counterpart in the replicative DNA polymerases, e.g., cellular pols δ and ε, and mitochondrial pol γ, and thus is a plausible target in the creation of selective inhibitors of pol β that might have relevance for drug design. Pol β has emerged as a potential target for combination chemotherapy with PARP inhibitors.[13,14] It is thus important to evolve structure-based approaches for the development of pol β probes and inhibitors.

We previously synthesized a series of dNTP analogues in which the β,γ-bridging oxygen is replaced with substituted methylene groups as probes of pol β active site structure and function. β,γ-dNTP analogues have been used to assess the influence of leaving group electrostatic charge and structure on the transition state for pol β, providing evidence of chemistry in the rate-determining step during turnover.[15,16] High-resolution crystal structures of pol β bound to a single-nucleotide gapped DNA substrate incubated with an ∼50:50 mixture of dGTP β,γ-substituted CXF diastereomers, where X is H, Cl, or CH_3, detected only one isomer, which in each case had the fluorine atom pointing toward the Arg183 residue.[17,18] In contrast, similar crystal structures of ternary complexes formed from β,γ-substituted CHCl-dGTP showed approximately equal occupancies for both isomeric forms in the active site of pol β.[17,18]

These observations pose several interesting questions. First, because a chemical reaction in the crystallized complex is difficult to follow kinetically, it would be useful to know whether a similar stereospecificity also occurs in free solution under pre-steady-state conditions and, if so, whether it is manifested in k_{pol} (transition-state effect), K_d (ground-state effect), or both. Second, in the case of the CXF isomer that was not detected in the active site by crystallography [i.e., (*S*)-CHF], it is important to establish whether the enzyme can use this isomer in the absence of the competing, preferred *R*-isomer and, if so, its relative rate of incorporation.

Received: July 31, 2012
Revised: October 4, 2012
Published: October 8, 2012

dx.doi.org/10.1021/bi3010335 | *Biochemistry* 2012, 51, 8491−8501

To address these questions, it was essential to have at our disposal the previously unknown individual CHF and CHCl-dGTP diastereomers, to know their absolute configurations (preferably bound into the active site complex of the enzyme), and to elaborate a method for analyzing them together or separately in solution during or after enzyme assays. The polymerase incorporation assays alone are inadequate because both the extended DNA and pCHXp (bisphosphonate, standing in for pyrophosphate from normal dNTPs) products from CHX diastereomer pairs are identical. The first examples of individual stereoisomers in this type of nucleotide analogue were recently prepared.[19] The four CHX (X is F or Cl) diastereomers described in this work were demonstrated to exhibit discrete ^{19}F and ^{31}P NMR spectra, allowing them to be distinguished unambiguously in solution, and all four gave single-ligand X-ray crystal structures with pol β, defining their absolute configurations in addition to their specific conformations within the active site, which proved to be very similar.[19] Thus, all the necessary tools were now at hand to determine whether the halogen substitution stereochemistry has any effect on binding (K_d) or the transition state (k_{pol}).

We first applied ^{19}F and ^{31}P NMR analysis[19] to determine the relative concentrations of unreacted (*R*)- and (*S*)-β,γ-CHF-dGTP in substrate diastereomer mixtures remaining in solution after some amount of pol β-catalyzed incorporation had occurred. The availability of the individual stereoisomers then allowed us to perform independent transient-state kinetic analyses to explore stereospecificity for correct incorporation opposite template C and misincorporation opposite T for the CHF- and CHCl-dGTP analogues. By comparing the wild-type (wt) pol β incorporation kinetics for the individual diastereomers with those of a mutant pol β in which Arg183 is replaced with alanine (R183A), we could also examine whether a specific electrostatic interaction between Arg183 and the fluorine atom is implicated in any observed stereospecificity for the *R*-isomer, which is relevant to assessing the potential of Arg183 as an element in the future design of selective pol β inhibitors.

MATERIALS AND METHODS

DNA Synthesis, Purification, Radiolabeling, and Annealing. Primer (5′-TAT TAC CGC GCT GAT GCG C), template (5′-GCG TTG TTC CGA CCC CCC GCG CAT CAG CGC GGT AAT A for NMR experiments or 5′-GCG TTG TTC CGA CMG CGC ATC AGC GCG GTA ATA, where M is C or T, for transient-state assays), and 5′-phosphorylated downstream (5′-GTC GGA ACA ACG C) oligomers were synthesized on a solid phase DNA synthesizer and purified by 16% denaturing polyacrylamide gel electrophoresis, followed by desalting using oligonucleotide purification cartridges. For the NMR analysis, 1 molar equiv of primer was mixed with 1.2 molar equiv of template, heated to 95 °C, and cooled slowly to room temperature to anneal the strands. For transient-state kinetic assays, 1 molar equiv of primer was 5′-end labeled with 0.4 unit/μL T4 polynucleotide kinase and 0.7 molar equiv of [γ-^{32}P]ATP with the supplied buffer at 37 °C for 30 min, followed by heat inactivation at 95 °C for 10 min. The primer was purified by size exclusion chromatography using a Bio-Spin 6 column and then annealed by mixing with 1.2 molar equiv of template and 1.5 molar equiv of downstream oligomers. The mixture was heated to 95 °C and cooled slowly to room temperature.

Protein, Reaction Buffer, and dGTP-β,γ-CHX Preparation. Wild-type and R183A mutant pol β were purified as previously reported.[20] The reaction buffer for all experiments consisted of 50 mM Tris-HCl, 20 mM KCl, 20 mM NaCl, 10 mM $MgCl_2$, 1 mM DTT, and 6% glycerol at pH 8.0 and 37 °C. Analogues (*R*/*S*)-β,γ-CHX-dGTP [X is F (**1a,b**), or X = Cl (**4a,b**)] were synthesized according to literature procedures.[16,18,19]

NMR Assay. Nine individual reaction tubes (100 μL final volume in each) containing 50 μM unlabeled and annealed primer/template were incubated with 100 μM wt pol β (final concentrations) in reaction buffer for 3 min at 37 °C, followed by addition of (*R*/*S*)-β,γ-CHF-dGTP to a final concentration of 1 mM (each diastereomer at 500 μM). The reactions were allowed to proceed for 5 h to incorporate up to 6 consecutive correct nt, and then the mixtures were heated to 95 °C for 10 min to melt the DNA. The reaction mixtures were pooled and centrifuged using a Microcon YM-3 column to exclude any reactants or products of >3 kDa. The pH of all NMR samples was adjusted to 9.8−10.0 with Na_2CO_3, and trace divalent metal ions were removed with Chelex-100. The resulting reaction mixture (500 μL) was then loaded into an NMR tube following insertion of a coaxial insert containing D_2O as an external reference. NMR spectra of compounds **1a** and **1b** before incorporation by pol β were obtained in D_2O with a net concentration of 10 mM. Spectra of the assay samples were obtained using an external D_2O reference, with a net concentration of the two diastereomers of ∼0.7 mM. The (*R*/*S*)-β,γ-CHCl-dGTP reactions were conducted in an identical fashion with the exception of reaction time, which was 8 h. A Wilmad coaxial insert (stem L 50 mm) was purchased from Sigma Aldrich. ^{19}F and ^{31}P NMR spectra were obtained on a Varian 400-MR two-channel NMR spectrometer. All chemical shifts are given on the δ scale in parts per million relative to external 85% H_3PO_4 (δ 0.00, ^{31}P NMR) and $CFCl_3$ (δ 0.00, ^{19}F NMR). ^{31}P NMR spectra were proton-decoupled. The signals of (*R*)-β,γ-CHF-dGTP and (*S*)-β,γ-CHF-dGTP diastereomers on ^{19}F and ^{31}P NMR spectra were assigned using the method of McKenna et al.[19]

NMR Settings. The ^{19}F NMR spectrum of dGTP-β,γ-CHF (**1a,b**) before incorporation by pol β was acquired using a Varian 400-MR default setting with a 75188 Hz sweep width and a −67773 Hz offset. ^{31}P NMR spectra of dGTP-β,γ-CHF (**1a,b**) and dGTP-β,γ-CHCl (**4a,b**) before incorporation by pol β were acquired using a Varian 400-MR default setting with a 4882 Hz sweep width, a 109 Hz offset, and a 0.30 Hz/point digital resolution. The ^{19}F NMR spectrum of the assay sample was acquired using a 4.600 μs pulse width, a 1.0 s relaxation delay, a 1.59 Hz/point digital resolution, a 52038 Hz sweep width, a −81878 Hz offset, a 0.63 s acquisition time, and 26000 acquisitions. ^{31}P NMR spectra of the assay samples were acquired using a 4.650 μs pulse width, a 1.0 s relaxation delay, a 0.30 Hz/point digital resolution, a 4882 Hz sweep width, a 109 Hz offset, a 3.36 s acquisition time, and 12000 acquisitions.

Transient-State Kinetic Analyses. Radiolabeled single-nucleotide gapped DNA (100 nM) was incubated with 600 nM pol β in reaction buffer (2× mixture) for 3 min at 37 °C. Equal volumes of the DNA/pol β mixture and a 2× solution of (*R*)-β,γ-CHX-dGTP or (*S*)-β,γ-CHX-dGTP at different concentrations were rapidly combined using a KinTek model RQF-3 quench-flow apparatus. After the appropriate reaction time, the reaction was quenched with 0.5 M EDTA (pH 8.0). Mixtures with reaction times longer than 20 s were mixed by hand. Reaction products were separated by 20% denaturing polyacrylamide gel electrophoresis (39 cm × 33 cm × 0.4 mm). Dehydrated gels were exposed to a phosphor screen and detected by

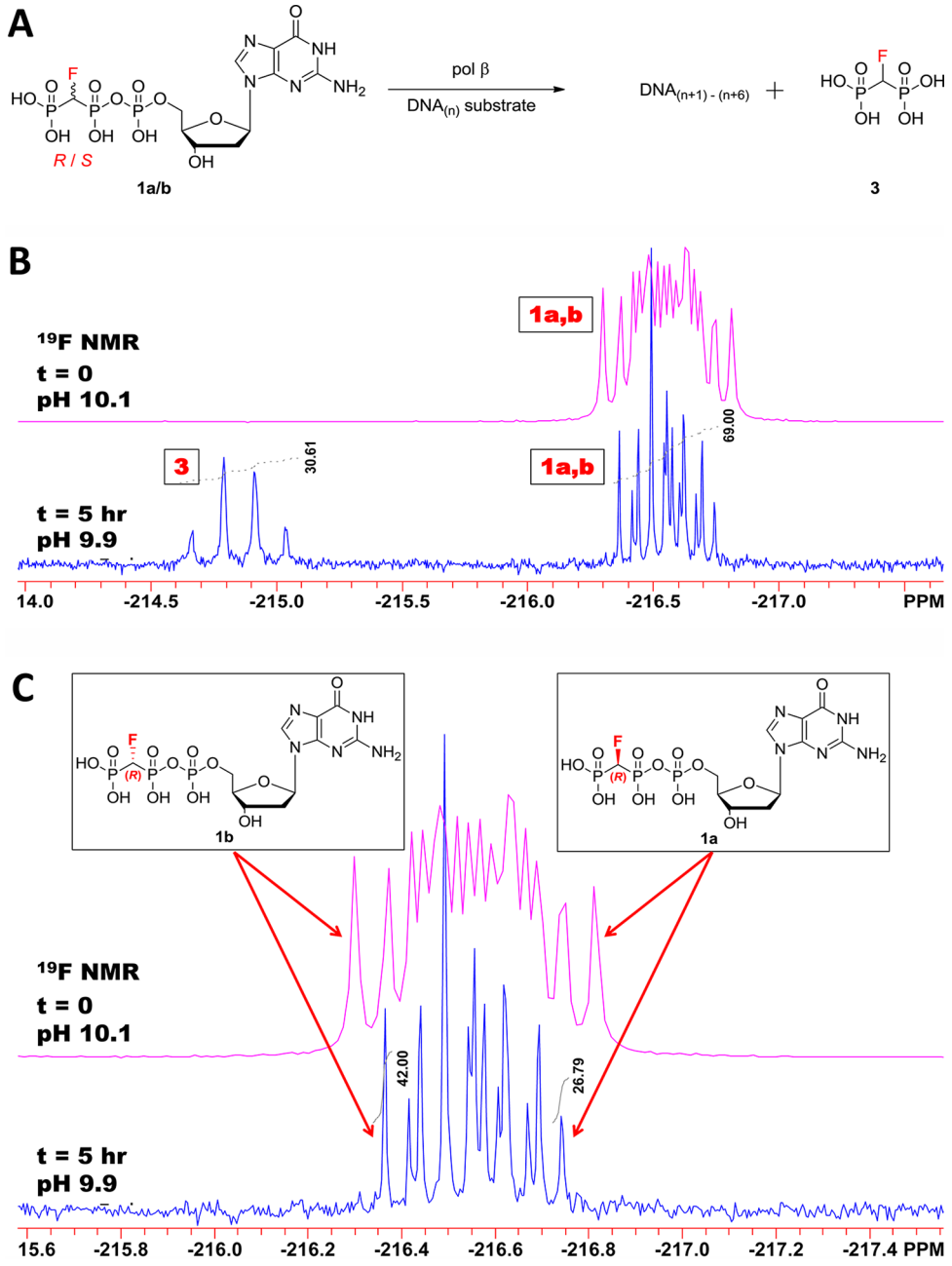

Figure 1. Reaction scheme and ^{19}F NMR spectra of reaction mixtures. (A) Sketch depicting the direct competition reaction conducted for the NMR analysis. β,γ-CHF-dGTP and p-CHF-p bisphosphonate are labeled below for identification with NMR spectra. $DNA_{(n+1)-(n+6)}$ denotes that up to 6 correct nt can be inserted opposite the 6 consecutive dCs in the template (see Materials and Methods). (B) β,γ-CHF-dGTP in an equal mixture of *R*- and *S*-stereoisomers was incubated with primer/template DNA with wt pol β, and ^{19}F NMR spectra were recorded at time zero (top pink trace) and after a 5 h incubation (bottom blue trace). Peaks are labeled as in panel A. (C) Close-up of peaks corresponding to the unreacted β,γ-CHF-dGTP analogue (**1a** and **1b**) at time zero (top pink trace) and after 5 h (bottom blue trace). The outer peaks can be used to specifically identify and quantitate the individual diastereomers, with the downfield (left) peak corresponding to the *S*-diastereomer (**1b**) and the upfield (right) peak corresponding to the *R*-diastereomer (**1a**). dGMP (**2**) from hydrolysis was < 2% by ^{31}P NMR (Figure S1 of the Supporting Information).

phosphorescence emission. All reactions were conducted in triplicate.

RESULTS

Preferential Insertion of (*R*)-CHF-dGTP from an ~1:1 Mixture of the *R*- and *S*-Diastereomers. Deoxyribonucleotide insertion by pol β was assessed by measuring the amounts of unreacted (*R*)- and (*S*)-CHF-dGTP remaining after the large-scale reaction had been terminated following the incorporation of up to 6 consecutive nt. Figure 1 shows ^{19}F NMR spectra of a reaction mixture consisting of DNA, wt pol β, and the *R*- and *S*-diastereomers of β,γ-CHF-dGTP present at approximately equimolar starting concentrations. The ^{19}F NMR spectra were recorded before and after a 5 h reaction with pol β as an offset overlay, with time zero (pink) above the reaction spectrum (blue). The same mixtures were used to obtain ^{31}P NMR spectra (Figure S1 of the Supporting Information), yielding data that are consistent with the ^{19}F NMR analysis. Figure 1B, which shows the entire region of interest in the ^{19}F NMR spectrum, allows calculation of the reaction progress based on the amount of

dx.doi.org/10.1021/bi3010335 | *Biochemistry* 2012, 51, 8491−8501

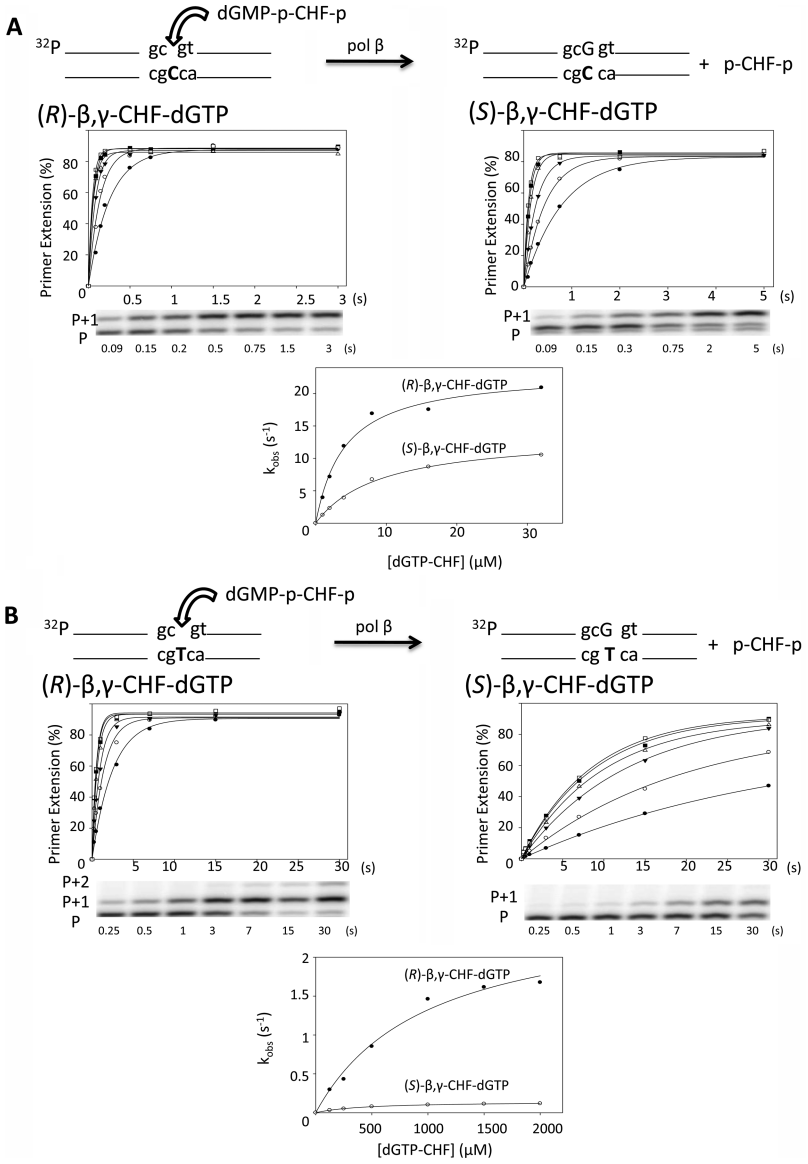

Figure 2. Pre-steady-state incorporation into single-gap DNA substrate reactions with separate CHF diastereomers. (A) Correct incorporation opposite dC of the *R*-diastereomer (left) and *S*-diastereomer (right). The plot of percentage primer extension vs time is shown for all six analogue concentrations [1 (●), 2 (○), 4 (▼), 8 (△), 16 (■), and 32 μM (□)], below which is a representative gel showing a time course with 1 μM analogue. The corresponding reaction time is shown below each lane. P represents the unextended primer and P + 1 the extension by a single dGMP. The observed rate constant is plotted opposite the corresponding analogue concentration for both the *R*- and *S*-analogues on the same plot for the purpose of comparison. (B) Misincorporation opposite dT of the *R*-diastereomer (left) and *S*-diastereomer (right). The plot of percentage primer extension vs time is shown for all six analogue concentrations [125 (●), 250 (○), 500 (▼), 1000 (△), 1500 (■), and 2000 μM (□)], below which is a representative gel showing a time course with 125 μM analogue. P represents the unextended primer, P + 1 the extension by a single dGMP, and P + 2 a second incorporation by displacement of the downstream oligonucleotide, which is observed for only the *R*-diastereomer. The corresponding reaction time is shown below each lane. The observed rate constant is plotted opposite the corresponding analogue concentration for both the *R*- and *S*-analogues on the same plot for the purpose of comparison. The reactions were conducted in triplicate and have a standard error of the mean of ±15%; the figure shows a representative data set.

fluoromethylenebisphosphonate (pCHFp) product observed relative to the amount of unreacted *β,γ*-CHF-dGTP remaining (peaks **3** and **1a,b**, respectively). Focusing on the remaining unreacted triphosphate analogue (Figure 1C), we find it is apparent that the two distal peaks can be assigned to individual diastereomers. The outside peak to the left is assigned to (*S*)-*β,γ*-CHF-dGTP and that to the right to (*R*)-*β,γ*-CHF-dGTP.[19]

After a 5 h incubation with primer/template DNA and pol *β*, the amount of *β,γ*-CHF-dGTP incorporated corresponds to nearly 30% utilization of the analogue, as revealed by integration of the bisphosphonate and nucleotide peaks in the ^{19}F NMR spectrum. From the ^{31}P NMR spectrum (Figure S1 of the Supporting Information), only 1.5% of the triphosphate analogue was converted to dGMP and bisphosphonate by a degradation process, as opposed to being incorporated into the DNA by pol *β*. Integration of the bisphosphonate and nucleotide peaks (Figure 1C) before and after reaction shows that both diastereomers must have been used, to account for the amount of bisphosphonate product formed, and that the relative consumption of isomers during the reaction occurred in a 3:1 (*R*:*S*) ratio (see the Supporting Information for a detailed description of the calculation). This experiment shows unequivocally that

dx.doi.org/10.1021/bi3010335 | *Biochemistry* 2012, 51, 8491−8501

Table 1. Pre-Steady-State Parameters for Correct and Incorrect Incorporation of (*R*)- and (*S*)-CHF and -CHCl Diastereomers by wt pol *β*[a]

pairing	diastereomer	k_{pol} (s^{-1})	K_d (μM)	stereospecificity
opposite C	(*R*)-CHF	18 ± 3	6.2 ± 2.2	3.8 ± 0.4
	(*S*)-CHF	9.2 ± 2.3	10 ± 1	
	(*R*)-CHCl	7.6 ± 1.2	3.2 ± 0.8	6.3 ± 0.8
	(*S*)-CHCl	4.8 ± 0.4	11 ± 1	
opposite T	(*R*)-CHF	2.3 ± 0.4	740 ± 140	11 ± 1
	(*S*)-CHF	0.16 ± 0.01	590 ± 110	
	(*R*)-CHCl	0.26 ± 0.01	290 ± 20	7.8 ± 0.4
	(*S*)-CHCl	0.051 ± 0.003	540 ± 30	

[a] k_{pol}, K_d, and stereospecificity values are reported as the mean ± the standard error of three replicates. Stereospecificity is defined as $(k_{pol}/K_d)_R/(k_{pol}/K_d)_S$.

(*S*)-*β*,*γ*-CHF-dGTP is also a substrate of pol *β* under these mixed stereoisomer conditions, despite not being detected[17,18] in a ternary complex structure by X-ray crystallographic analysis, formed by exposure of binary DNA pol *β*−ddCTP−DNA crystals to solutions of the mixed stereoisomers.

Kinetics of Individual (*R*)- and (*S*)-*β*,*γ*-CHF-dGTP Diastereomer Utilization. The DNA incorporation reactions of the individual (*R*)- and (*S*)-*β*,*γ*-CHF-dGTP diastereomers catalyzed by pol *β* were analyzed using quench-flow transient-state kinetic assays. For each diastereomer, exponential time courses with different analogue concentrations were determined to measure the correct incorporation opposite dC (Figure 2A) and misincorporation opposite dT (Figure 2B). The percentage of primer extended is plotted versus time, and the datum for each concentration is fit to the first-order exponential $y = a(1 - e^{-kt})$, where a is the maximal percent of primer extension and k is the observed rate constant. The observed rate constant (k_{obs}) is plotted versus the corresponding analogue concentration, and the data fit to the rectangular hyperbola $k_{obs} = k_{pol}[\beta,\gamma\text{-CHF-dGTP}]/(K_d + [\beta,\gamma\text{-CHF-dGTP}])$ to give the k_{pol} and K_d parameters (Figure 2 and Table 1). The stereospecificity (*S*) is given by the k_{pol}/K_d ratios for the stereoisomers; $S = (k_{pol}/K_d)_R/(k_{pol}/K_d)_S$ (Table 1). Both dGTP diastereomers were incorporated opposite dC in the single-nucleotide gapped DNA substrate, visualized as the addition of a single deoxynucleotide to the 3′-end of the primer strand (Figure 2A, P+1 PAGE band). The *R*-diastereomer was incorporated with a 2-fold larger k_{pol} and a 1.5-fold smaller apparent K_d than the *S*-diastereomer, resulting in an *S* of 3.8 (Table 1), which agrees with the *S* of 3 obtained by NMR, within the estimated error. The agreement between the NMR and kinetic methods indicates that DNA polymerase substrate specificity measured with two dNTPs competing directly for incorporation into DNA is equivalent to using kinetics to determine specificity by measuring k_{pol}/K_d values for dNTP substrates in separate reactions[21] and is in accord with a model by Fersht.[22]

Elevated concentrations of (*R*)- and (*S*)-*β*,*γ*-CHF-dGTP substrates (125−2000 μM) were used to measure misincorporation opposite template T (Figure 2B, P + 1 and P + 2 PAGE bands). The formation of mispairs opposite T shows a much larger disparity between the catalytic rates for the *R*- and *S*-diastereomers ($k_{pol,R}/k_{pol,S} \sim 14.4$) versus that observed for incorporation opposite C ($k_{pol,R}/k_{pol,S} \sim 2.0$), whereas the overall apparent binding constants were similar (i.e., within a factor of 2), for incorporations opposite either C or T (Figure 2 and Table 1). The P + 2 gel band (Figure 2B, left-hand gel) represents a correct incorporation opposite the downstream C occurring via strand displacement at the high substrate concentrations required for the detection of misincorporation.

The (*S*)-*β*,*γ*-CHF-dGTP "missing" from the ternary crystal structure obtained using the diastereomer mix[17,18] was observed in the crystal structure using the individual *S*-diastereomer alone.[19] The ternary crystal structure obtained with the individual *R*-isomer showed it in the same active site location found using the mixture of the *R*- and *S*-diastereomers, with the fluorine atom pointed toward Arg183.[17,18] The new structure containing the *S*-diastereomer was observed to overlay closely with the *R*-diastereomer, but with F pointing away from Arg183. The F atom in the *R*-diastereomer was 3.1 Å from a nitrogen atom of Arg183, suggesting the possibility of an F−guanidinium (Arg183) electrostatic interaction.

High-resolution ternary complex structures with pol *β* bound to single-nucleotide gapped DNA in the presence of *β*,*γ*-substituted dGTP analogues CHCl, CHBr, and CHMe contained both *R*- and *S*-diastereomers in approximately equal amounts. In contrast, the structures obtained using *β*,*γ*-CXF-dGTP analogues contained the *R*-diastereomer.[17] Increased stability afforded by F atoms in the *R*-configuration interacting with Arg183 in pol *β* might favor crystal complex formation versus the *S*-diastereomer. When both diastereomers are present, the specificity need be only ∼3,[17,18] consistent with the small K_d effects seen in solution.

Preferential Insertion of (*R*)-CHCl- over (*S*)-CHCl-dGTP from a Diastereomeric Mixture by Pol *β*. Figure 3 shows the ^{31}P NMR spectra of a reaction mixture consisting of primer/template DNA, pol *β*, and (*R*/*S*)-*β*,*γ*-CHCl-dGTP, where the *R*- and *S*-diastereomers are present at equimolar starting concentrations. The top (pink) spectrum was obtained before the reaction, and the bottom (blue) spectrum was the same mixture after an 8 h incubation at 37 °C. Reaction progress was determined by dividing the integral of the bisphosphonate peak at ∼13 ppm (compound **5**, and labeled as such on spectra) by 2, due to the two P atoms in the bisphosphonate molecule, and is calculated to be 27% (Figure 3B). From the observation of P_α resonances (Figure 3C), the relative consumption of the *R*- and *S*-diastereomers can be calculated; the leftmost peak is attributed solely to the *S*-diastereomer and the rightmost one solely the to the *R*-diastereomer, as discussed above. The diastereomers were consumed during the reaction in a 7:1 (*R*:*S*) ratio. See Figure S2 of the Supporting Information for a close-up of the P_β signals that yield the same result. Approximately 3% of the initial analogue in the reaction mixture was decomposed into dGMP and chloromethylenebisphosphonate, pCHClp (Figure 3B, compound and peak **2**).

dx.doi.org/10.1021/bi3010335 | *Biochemistry* 2012, 51, 8491−8501

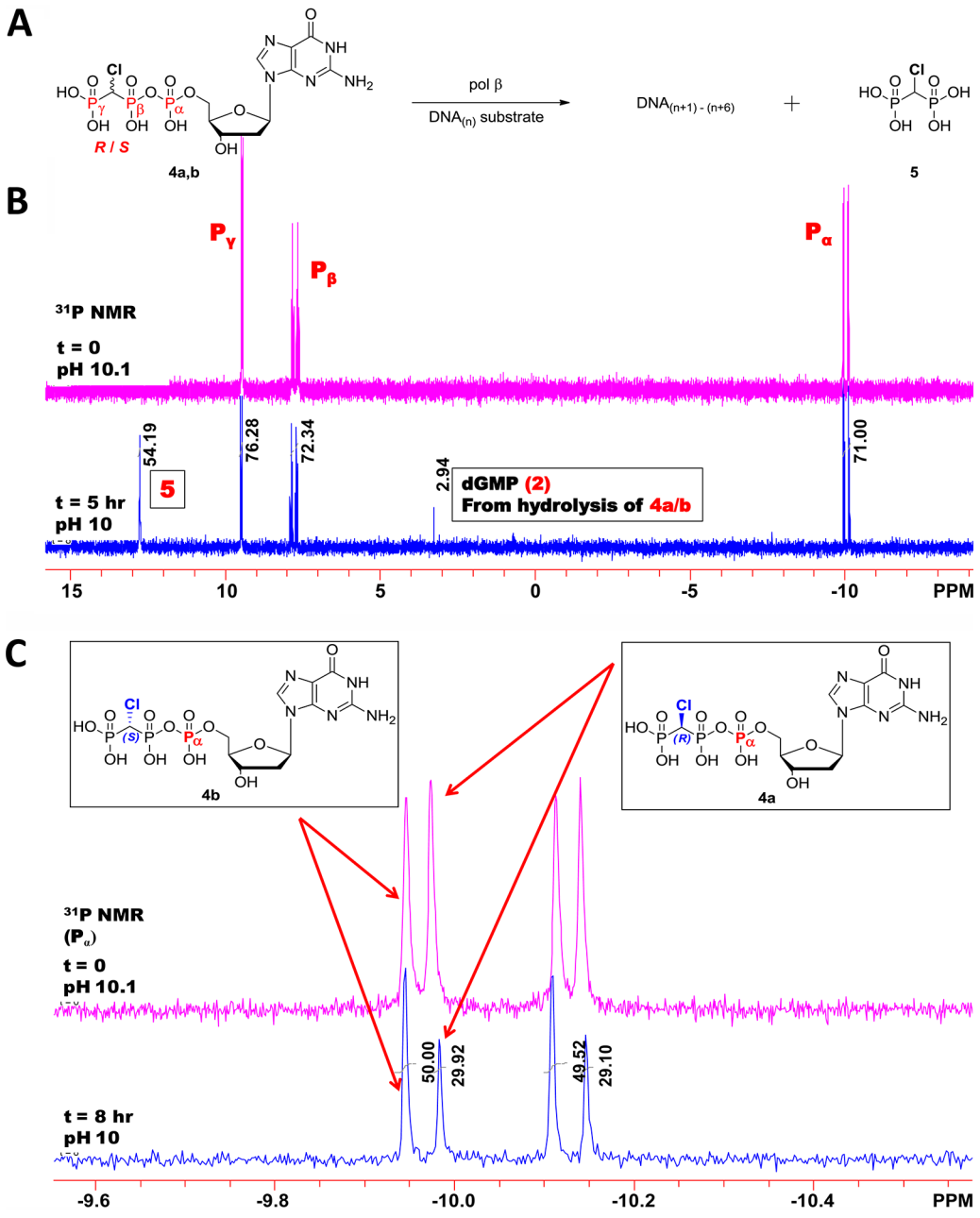

Figure 3. Reaction scheme and ^{31}P NMR spectra of (*R*/*S*)-*β*,*γ*-CHCl-dGTP reaction mixtures. (A) Reaction scheme depicting the direct competition between (*R*)-*β*,*γ*-CHCl-dGTP and (*S*)-*β*,*γ*-CHCl-dGTP for incorporation into DNA by wild-type pol *β*. Phosphorus atoms of (*R*/*S*)-*β*,*γ*-CHCl-dGTP and p-CHCl-p bisphosphonate are labeled for reference in the NMR spectra. $DNA_{(n+1)-(n+6)}$ denotes that up to 6 correct nt can be inserted opposite the 6 consecutive dCs in the template (see Materials and Methods). (B) Primer/template DNA was incubated with wt pol *β* and (*R*/*S*)-*β*,*γ*-CHCl-dGTP in a 50:50 *R*:*S* mixture. ^{31}P NMR spectra were taken at time zero (top pink trace) and after an 8 h incubation at 37 °C (bottom blue trace) following treatment as described in Materials and Methods. Peaks are labeled as in panel A. (C) Close-up of the region of interest around P_α. The leftmost peak is due to (*S*)-*β*,*γ*-CHCl-dGTP (**4b**) alone, while the peak at approximately −10 ppm is due to (*R*)-*β*,*γ*-CHCl-dGTP (**4a**) alone.

Pre-Steady-State Kinetics with Separated (*R*)-CHCl and (*S*)-CHCl Diastereomers. The individual (*R*)- and (*S*)-*β*,*γ*-CHCl-dGTP diastereomers were used as substrates in pre-steady-state assays with pol *β* (Figure 4). As with the fluorine analogues, time courses were determined at six concentrations of each substrate for correct incorporation opposite dC (Figure 4A) and misincorporation opposite dT (Figure 4B). The data were plotted and analyzed in the same way as with the fluorine analogues. The values of k_{pol} and K_d are listed in Table 1.

As observed in the NMR experiment, both diastereomers are incorporated by pol *β*; however, the diastereomer with the chlorine atom oriented toward the R183 residue (*R*) is incorporated with a slight catalytic advantage (7.6 s^{-1} vs 4.8 s^{-1}) and an apparent binding constant ~3-fold lower (3.2 *μ*M) than that of the *S*-diastereomer (11 *μ*M) (Table 1). The stereospecificity ratio $[(k_{pol}/K_d)_R/(k_{pol}/K_d)_S]$ of 6.3 is in agreement with the value of 7 obtained using the NMR method. Therefore, the observed relative incorporation of (*R*)-CHCl over (*S*)-CHCl is slightly larger than the approximate detection limit for the distribution of each diastereomer in the tertiary crystal structure, which showed equal populations of (*R*)-CHCl and (*S*)-CHCl.[17]

dx.doi.org/10.1021/bi3010335 | *Biochemistry* 2012, 51, 8491−8501

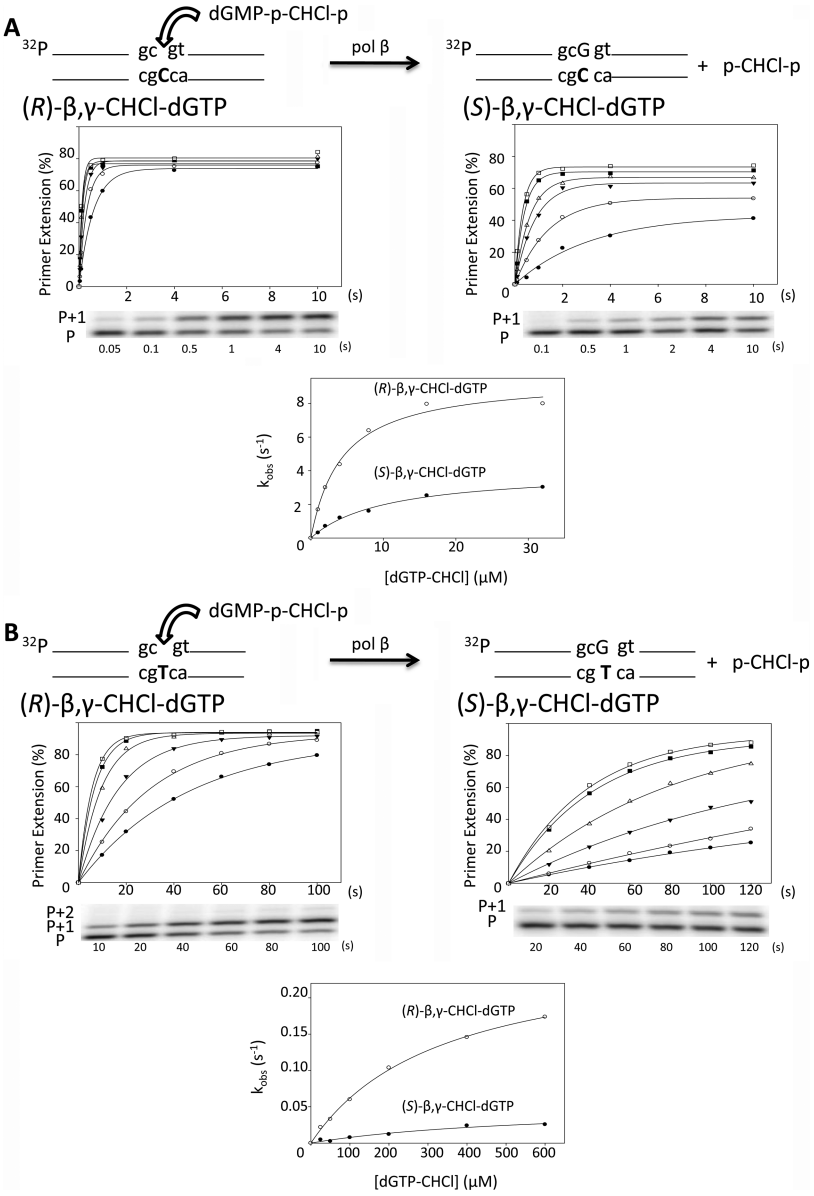

Figure 4. Pre-steady-state incorporation of (*R*/*S*)-*β*,*γ*-CHCl-dGTP into single-gapped DNA. (A) Correct incorporation opposite dC of (*R*)-CHCl (left) and (*S*)-CHCl (right). The cartoon shows the generalized scheme for the reaction. A plot of the percentage of primer extension vs time for six concentrations of the CHCl analogue is shown for one of three repeats of each reaction [1 (●), 2 (○), 4 (▼), 8 (△), 16 (■), and 32 μM (□)]. Below each plot is a time course shown on a representative gel for the first concentration (1 μM), where P represents the unextended primer and P + 1 the extension of the primer by a single incorporation. The corresponding reaction time is shown below each lane. Below these gels is a plot of the observed rate constant vs the corresponding analogue concentration for both diastereomers. (B) Misincorporation opposite dT of (*R*)-CHCl (left) and (*S*)-CHCl (right). As for the correct pairing, the percentage of primer extension vs time for each concentration of analogue is shown for both diastereomers [25 (●), 50 (○), 100 (▼), 200 (△), 400 (■), and 600 μM (□)] with a representative gel for each set of reactions; the corresponding reaction time is shown below each lane. The observed rate constant is plotted vs the corresponding analogue concentration on the same plot for each diastereomer below. The reactions were conducted in triplicate and have a standard error of the mean of ±15%; the figure shows a representative data set.

Kinetic Analysis of Stereoisomeric Substrates with the R183A Mutant of Pol *β*. To examine further the hypothesis of a specific bonding interaction between the fluorine atom of the *R*-diastereomer and the guanidinium group of Arg183, we repeated the kinetic analysis with the separate (*R*)- and (*S*)-CHF diastereomers using a pol *β* mutant in which Arg183 was replaced with alanine (Figure 5). No measurable difference was found between the catalytic insertion rate constants for the separate diastereomers ($k_{pol,R}$ = 0.27 s^{-1}; $k_{pol,S}$ = 0.29 s^{-1}), while there is a significant relative reduction in the apparent binding constant of the *S*-diastereomer ($K_{d,R}$ = 6.8 μM; $K_{d,S}$ = 39 μM) (Table 2). The overall stereospecificity favoring the incorporation of the *R*-diastereomer has been increased by ∼1.5-fold for the mutant polymerase, stemming principally from a sizable (∼6-fold) destabilization in the binding of the *S*-isomer relative to that of the *R*-isomer, which may suggest a local repulsive effect.

For the Cl diastereomers, a specificity difference between the (*R*)-CHCl and (*S*)-CHCl diastereomers remains when R183 is replaced with Ala (Figure 5B and Table 2). The difference between the *R*- and *S*-diastereomers in both the catalytic rate constant (∼2-fold) and K_d (∼3-fold) remains the same for both the wt and R183A mutant pol *β* (Table 2).

dx.doi.org/10.1021/bi3010335 | *Biochemistry* 2012, 51, 8491−8501

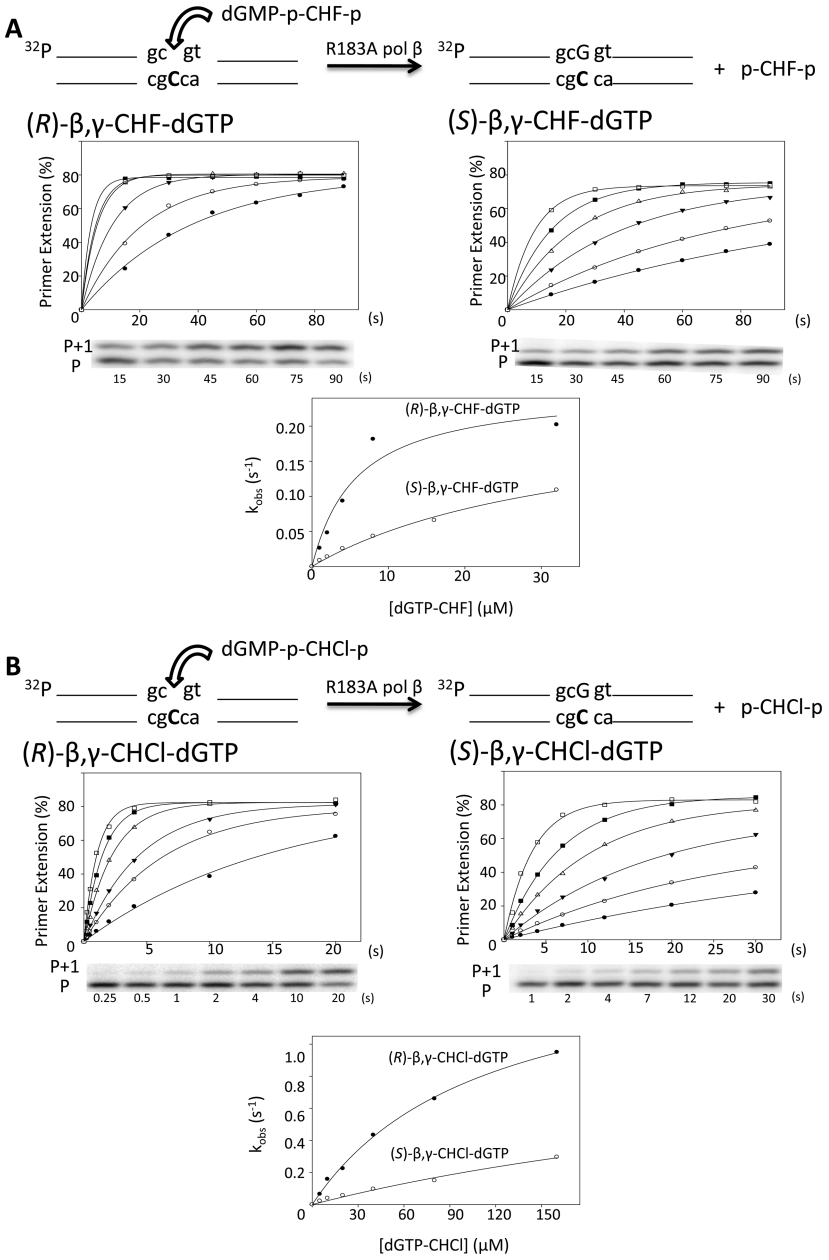

Figure 5. Pre-steady-state incorporation by R183A pol β into single-gap DNA substrate reactions with separate diastereomers. (A) Correct incorporation opposite dC of (*R*)-β,γ-CHF-dGTP (left) and (*S*)-β,γ-CHF-dGTP (right) diastereomers. The plot of percentage primer extension vs time is shown for all six analogue concentrations [1 (●), 2 (○), 4 (▼), 8 (△), 16 (■), and 32 μM (□)], below which is a representative gel showing a time course with 1 μM analogue. P represents the unextended primer and P + 1 the extension by a single dGMP. The corresponding reaction time is shown below each lane. The observed rate constant is plotted opposite the corresponding analogue concentration for both the *R*- and *S*-analogues on the same plot for the purpose of comparison. (B) Correct incorporation opposite dC of (*R*)-β,γ-CHCl-dGTP (left) and (*S*)-β,γ-CHCl-dGTP (right) by R183A pol β. The plot of percentage primer extension vs time is shown for each analogue concentration [5 (●), 10 (○), 20 (▼), 40 (△), 80 (■), and 160 μM (□)] with a representative gel picture underneath; the corresponding reaction time is shown below each lane. The observed rate constant is plotted vs the corresponding analogue concentration below. The reactions were conducted in triplicate and have a standard error of the mean of ±15%; the figure shows a representative data set.

■ DISCUSSION

In a recent review, Stahl et al.[23] usefully surveyed the phenomena of molecular interactions between ligands and receptors from the perspective of structure-based drug design, in which the medicinal chemist attempts to identify, inventory, and optimize specific contributions of such interactions in the ground state to rationalize and enhance the overall binding affinity of, for example, an inhibitor for the enzyme site to which it binds. The authors emphasize the limitations and constraints imposed on attempts to map binding free energies to an analysis of three-dimensional structures, noting the difficulties encountered in correlating interactions observed in static ligand−protein complex structures with solution affinities.[23]

Nevertheless, it is well recognized that so-called weak hydrogen bonds between a covalently bound F atom in the ligand and a polar hydrogen atom HX (X is O or N) in the protein active site are frequently found in the Protein Data Bank,[23] and introduction of such interactions by design has been

dx.doi.org/10.1021/bi3010335 | *Biochemistry* 2012, 51, 8491−8501

Table 2. Pre-Steady-State Parameters for Correct Incorporation of (*R*)- and (*S*)-CHF and -CHCl Diastereomers by R183A pol β[a]

diastereomer	k_{pol} (s^{-1})	K_d (μM)
(*R*)-CHF	0.27 ± 0.02	6.8 ± 1.0
(*S*)-CHF	0.29 ± 0.06	39 ± 8
(*R*)-CHCl	1.5 ± 0.1	110 ± 3
(*S*)-CHCl	0.88 ± 0.13	300 ± 96

[a] k_{pol} and K_d values are reported as the mean ± the standard error of three replicates.

associated with increased ligand affinity.[23] Weak interactions of Cl and higher halogens with both electrophiles and nucleophiles have also been widely documented under the omnibus rubric of "halogen bonds" and in some instances can enhance binding of the halo-substituted ligand to a receptor site.[23] All the more challenging with respect to these considerations is the task of achieving a fundamental understanding of enzyme catalysis and specificity in terms of active site complex structures where multiple hydrophobic, electrostatic, and steric interactions may contribute to an observed effect, and which requires the application of sophisticated transition-state theory supported by powerful computational tools.[24,25]

With these caveats in mind, we believe that our results allow several interesting conclusions. First, the precise placement of the CHX F or Cl atom in the active site of DNA pol β as determined by the choice of diastereomer can influence the energy of the transition state during turnover, particularly for the G·T mispair, as well as that of the ground state. Moreover, the fact that the diastereomers have congruent conformations in the preorganized bound state suggests that these compounds represent a novel "testing bed" for pairwise comparisons of CHX interactions within the active site, because the strong electrostatic bonding and other bonding of the "triphosphate" and sugar−base components largely predetermine the conformation of the nucleotide in the site, fixing the orientations in the two isomers of the C-X substituents and thereby creating a unique system for studying weak interactions of the latter with the protein (which may also affect neighboring PO oxygen atoms).

Second, we previously synthesized a series of dNTP analogues having the β,γ-bridging oxygen replaced by a series of monohalo, dihalo, halo-methyl, azido-methyl, dimethyl, and unsubstituted methylene groups.[17,19,26,27] These compounds, comprising a "toolkit" currently with more than a dozen members, span a broad range of leaving group (bisphosphonic acid) pK_{a4} values: 7.8 (CF_2) to 12.3 (CMe_2). Because of the widely different electronic and, in some instances, steric properties of the bisphosphonate moieties, the analogues are sensitive probes of deoxynucleotide incorporation and fidelity mechanisms for DNA polymerases (we are currently exploring the ability of the probes to act as substrates for other polymerases). In the case of pol β, analogues are incorporated in accord with linear free energy relationships (LFER) between log k_{pol} and pK_{a4} that have negative slopes for dG versus dC and dG versus dT, thus affirming that the insertion (chemical) step (k_{pol}) is rate-limiting for both correct (Watson−Crick) and incorrect (non-Watson−Crick base pairs) catalysis.[15,16,28−31] In these experiments, the CXY analogues in which X ≠ Y could be tested only as the diastereomeric mixtures obtained by conventional synthetic procedures. For CHF and CHCl, the *R*:*S* ratio data now obtained for the individual diastereomers show that the mixed diastereomers' averaged k_{pol} values are fair approximations with contributions from both isomers.

Third, we previously found that soaking DNA binary complex crystals of pol β with a 1:1 mixture of β,γ-CHF-dGTP diastereomers resulted in a ternary complex with only (*R*)-β,γ-CHF-dGTP being observable. The estimated limit of detection for occupancy by the alternate stereoisomer suggested, approximately, a stereopreference of >3; i.e., (*S*)-β,γ-CHF might not be detected in the crystal if (*S*)-β,γ-CHF is ≤25% present. In contrast, with β,γ-CHCl-dGTP, both isomers detectably populated the active site. We have now shown by NMR analysis of the pol β-dependent reaction with the diastereomeric mixture that (*S*)-β,γ-CHF-dGTP is utilized with approximately one-third of the efficiency of the *R*-diastereomer (Figure 1). Kinetic results obtained with the separately synthesized diastereomers showed a 3.8-fold more efficient incorporation of (*R*)-β,γ-CHF-dGTP compared to the *S*-isomer (Table 1), in reasonable agreement with the indirect NMR measurements. Thus, the position of the fluorine atom must modulate the free energy of the transition state relative to that of the ground state.

Native pol β incorporates (*R*)-CHF with a 2-fold higher k_{pol} (Table 1). The structural data obtained with the *R*- and *S*-diastereomer mixture and with the separated *R*-diastereomer showed that the fluorine atom in the *R*-configuration is 3.1 Å from a nitrogen atom of Arg183. The fluorine atom points away from Arg183 in the enzyme complex structure obtained with the separated *S*-diastereomer. The proximity of the (*R*)-fluorine atom to Arg183 suggests that the discrimination in k_{pol} favoring *R* over *S* reflects a specific polar interaction between the fluorine atom and the guanidinium moiety of Arg183. Replacing Arg with Ala should eliminate any electrostatic interaction present, although it may replace it with a weak hydrophobic interaction, which is a known capability of the CF group.[23] The kinetic data support a weak electrostatic interaction between the (*R*)-fluorine atom and Arg183 because the R183A mutant pol β incorporates both *R*- and *S*-stereoisomers with almost identical values of k_{pol} (Table 2).

Next, the proximity of *R*-CHF to Arg183 prompts us to add new fuel to the longstanding and ongoing controversy over whether CF can form H-bonds.[32−35] Studies of organic halides (principally the CF group) have suggested that these are very weak hydrogen bond acceptors.[23,32,36] Although a differentiation in terminology between hydrogen bond formation and dipolar interaction might be viewed as being largely semantic, particularly because hydrogen bonding also has a dominant electrostatic component, there is clearly a conceptual issue stemming from the fact that hydrogen bonding also has a covalent component, whereas dipolar interactions by definition are purely electrostatic. In our study, the evidence of an electrostatic (dipolar) interaction between *R*-F and the guanidinium moiety is persuasive (Tables 1 and 2); however, the 3.1 Å distance between *R*-F and Arg183 is clearly compatible with typical H-bonding distances.[37] Dalvit and Vulpetti[32,36] have proposed an empirical correlation between the ^{19}F shifts and F−H interactions, in part using some of our own previously published data.[17,18] Perhaps a computational analysis using an empirical valence bond treatment[38] could provide insight into whether an H-bond is formed. As mentioned above, because the nucleotide is held in place within the active site by strong charge interactions ("preorganization"), the resulting complex offers an intriguing new system for evaluating the strength and origins of weak F-bonds in enzyme active sites.

dx.doi.org/10.1021/bi3010335 | *Biochemistry* 2012, 51, 8491−8501

Dalvit and Vulpetti have proposed a "rule of shielding" for drug design to utilize fluorinated moieties to enhance binding affinities, based on a proposed empirical correlation between the fluorine isotropic chemical shifts and their interactions with proteins observed in crystal structures.[32,36] This empirical correlation suggested that shielded fluorines are found in close contact with hydrogen bond donors, whereas deshielded fluorines are often found to be near hydrophobic side chains or a backbone carbonyl, consistent with a dual character of fluorine as a potential hydrogen bond acceptor (or dipolar interaction partner) and a hydrophobic group. Our CHF analogues exhibit a ^{19}F chemical shift of −216 ppm, indicating strong shielding at the F atom, consistent with a disposition to act as a hydrogen bonding acceptor.

Despite the observed equal populations of (*R*)- and (*S*)-*β*,*γ*-CHCl-dGTP in the tertiary crystal structure obtained with the diastereomer mixture, pol *β* incorporates the *R*-isomer 7-fold more efficiently than the *S*-isomer (Figure 3) and binds the *R*-isomer approximately 3-fold better (Table 1). This "discrepancy" between the crystallography and the kinetic data cannot be explained simply by a detection limitation in the crystallography technique and has been verified by both NMR and pre-steady-state kinetic measurements [*S* = 6.3 (Table 1)]. The stereospecificity is not caused solely by an interaction between the Cl atom of the *R*-isomer and the guanidinium group of R183, because there is still a significant difference between the k_{pol} values for the *S*- and *R*-isomers incorporated by the R183A mutant of pol *β* (Figure 5 and Table 2) (see below). A detailed explanation of the observed effects will require information about the structure of the transition state, differences between the crystal and solution complexes, and should account for any possible C−X interactions with nearby PO oxygens.

The frequent occurrence of interactions between CF and polar H-atoms has been mentioned. The other halogens (Cl, Br, and I) sometimes have significant interactions with carbonyl groups or other classical H-bond acceptors, which are collectively termed "halogen bonds".[23] Such interactions have been verified by structural and structure−activity relationship (SAR) data.[23] Although halogen bonds formed by chlorine are typically weak, they can play a unique role in some complexes, i.e., triclosan, a broad-spectrum bactericide containing a chlorine atom interacting at a distance of 3.3−3.5 Å with a backbone carbonyl in the FabI active site. Replacement of the chlorine atom with lipophilic or hydrogen bonding substituents did not lead to compounds with higher potencies.[23]

Regardless of their details, the evidence provided by our kinetics studies for the importance of CHX stereochemistry in *β*,*γ*-CXY-dGTP substrates of pol *β* under dynamic, turnover conditions gives further support for an intriguing translational opportunity. Pol *β* has generated considerable interest as a target for the development of inhibitors based on its overriding importance in single-nucleotide BER[1,2] and its implied role in cancer.[3−12] Arg183 in pol *β* could be a unique active site target for selective inhibition based on its unique role in family X DNA polymerases.

■ ASSOCIATED CONTENT

Supporting Information

^{31}P NMR spectrum of CHF reactions (Figure S1), ^{31}P NMR spectrum of P_β from CHCl reactions (Figure S2), and a detailed description of the relative use calculation from the NMR experiments. This material is available free of charge via the Internet at http://pubs.acs.org.

■ AUTHOR INFORMATION

Corresponding Author

*Telephone: (213) 740-5190. Fax: (213) 740-8631. E-mail: mgoodman@usc.edu.

Funding

This research was supported, in part, by the National Cancer Institute of the National Institutes of Health via Grant 5-U19-CA105010, by the National Institutes of Health via Grant R01-GM21422 (to M.F.G.) and by Research Project Numbers Z01-ES050158 and Z01-ES050159 from the Intramural Research Program of the National Institutes of Health, National Institute of Environmental Health Sciences.

Notes

The authors declare no competing financial interests.

■ REFERENCES

(1) Matsumoto, Y., and Kim, K. (1995) Excision of deoxyribose phosphate residues by DNA polymerase *β* during DNA repair. *Science 269*, 699−702.

(2) Piersen, C. E., Prasad, R., Wilson, S. H., and Lloyd, R. S. (1996) Evidence for an imino intermediate in the DNA polymerase *β* deoxyribose phosphate excision reaction. *J. Biol. Chem. 271*, 17811−17815.

(3) Srivastava, D. K., Husain, I., Arteaga, C. L., and Wilson, S. H. (1999) DNA polymerase *β* expression differences in selected human tumors and cell lines. *Carcinogenesis 20*, 1049−1054.

(4) Bhattacharyya, N., Chen, H. C., Comhair, S., Erzurum, S. C., and Banerjee, S. (1999) Variant forms of DNA polymerase *β* in primary lung carcinomas. *DNA Cell Biol. 18*, 549−554.

(5) Bhattacharyya, N., Chen, H. C., Grundfest-Broniatowski, S., and Banerjee, S. (1999) Alteration of hMSH2 and DNA polymerase *β* genes in breast carcinomas and fibroadenomas. *Biochem. Biophys. Res. Commun. 259*, 429−435.

(6) Dobashi, Y., Shuin, T., Tsuruga, H., Uemura, H., Torigoe, S., and Kubota, Y. (1994) DNA polymerase *β* gene mutation in human prostate cancer. *Cancer Res. 54*, 2827−2829.

(7) Dong, Z., Zhao, G., Zhao, Q., Yang, H., Xue, L., Tan, X., and Zheng, N. (2002) A study of DNA polymerase *β* mutation in human esophageal cancer. *Zhonghua Yi Xue Za Zhi 82*, 899−902.

(8) Iwanaga, A., Ouchida, M., Miyazaki, K., Hori, K., and Mukai, T. (1999) Functional mutation of DNA polymerase *β* found in human gastric cancer: Inability of the base excision repair in vitro. *Mutat. Res. 435*, 121−128.

(9) Matsuzaki, J., Dobashi, Y., Miyamoto, H., Ikeda, I., Fujinami, K., Shuin, T., and Kubota, Y. (1996) DNA polymerase *β* gene mutations in human bladder cancer. *Mol. Carcinog. 15*, 38−43.

(10) Miyamoto, H., Miyagi, Y., Ishikawa, T., Ichikawa, Y., Hosaka, M., and Kubota, Y. (1999) DNA polymerase *β* gene mutation in human breast cancer. *Int. J. Cancer 83*, 708−709.

(11) Starcevic, D., Dalal, S., and Sweasy, J. B. (2004) Is there a link between DNA polymerase *β* and cancer? *Cell Cycle 3*, 998−1001.

(12) Wang, L., Patel, U., Ghosh, L., and Banerjee, S. (1992) DNA polymerase *β* mutations in human colorectal cancer. *Cancer Res. 52*, 4824−4827.

(13) Horton, J. K., and Wilson, S. H. (2007) Hypersensitivity phenotypes associated with genetic and synthetic inhibitor-induced base excision repair deficiency. *DNA Repair 6*, 530−543.

(14) Madhusudan, S., and Middleton, M. R. (2005) The emerging role of DNA repair proteins as predictive, prognostic and therapeutic targets in cancer. *Cancer Treat. Rev. 31*, 603−617.

(15) Sucato, C. A., Upton, T. G., Kashemirov, B. A., Batra, V. K., Martinek, V., Xiang, Y., Beard, W. A., Pedersen, L. C., Wilson, S. H., McKenna, C. E., Florian, J., Warshel, A., and Goodman, M. F. (2007) Modifying the *β*,*γ* leaving-group bridging oxygen alters nucleotide incorporation efficiency, fidelity, and the catalytic mechanism of DNA polymerase *β*. *Biochemistry 46*, 461−471.

(16) Sucato, C. A., Upton, T. G., Kashemirov, B. A., Osuna, J., Oertell, K., Beard, W. A., Wilson, S. H., Florian, J., Warshel, A., McKenna, C. E., and Goodman, M. F. (2008) DNA polymerase β fidelity: Halomethylene-modified leaving groups in pre-steady-state kinetic analysis reveal differences at the chemical transition state. *Biochemistry 47*, 870–879.
(17) Batra, V. K., Pedersen, L., Beard, W. A., Wilson, S. H., Kashemirov, B. A., Upton, T., Goodman, M. F., and McKenna, C. E. (2010) Halogenated β,γ-methylene- and ethylidene-dGTP-DNA ternary complexes with DNA polymerase β: Structural evidence for stereospecific binding of the fluoromethylene analogues. *J. Am. Chem. Soc. 132*, 7617–7625.
(18) McKenna, C. E., Kashemirov, B. A., Upton, T., Batra, V. K., Goodman, M. F., Pedersen, L., Beard, W. A., and Wilson, S. H. (2007) (R)-β,γ-fluoromethylene-dGTP-DNA ternary complex with DNA polymerase β. *J. Am. Chem. Soc. 129*, 15412–15413.
(19) Wu, Y., Zakharova, V. M., Kashemirov, B. A., Goodman, M. F., Batra, V. K., Wilson, S. H., and McKenna, C. E. (2012) β,γ-CHF- and β,γ-CHCl-dGTP Diastereomers: Synthesis, Discrete ^{31}P NMR Signatures, and Absolute Configurations of New Stereochemical Probes for DNA Polymerases. *J. Am. Chem. Soc. 134*, 8734–8737.
(20) Beard, W. A., and Wilson, S. H. (1995) Purification and domain-mapping of mammalian DNA polymerase β. *Methods Enzymol. 262*, 98–107.
(21) Bertram, J. G., Oertell, K., Petruska, J., and Goodman, M. F. (2010) DNA polymerase fidelity: Comparing direct competition of right and wrong dNTP substrates with steady state and pre-steady state kinetics. *Biochemistry 49*, 20–28.
(22) Fersht, A. R. (1985) *Enzyme Structure and Mechanism*, 2nd ed., W.H. Freeman & Co., New York.
(23) Bissantz, C., Kuhn, B., and Stahl, M. (2010) A Medicinal Chemist's Guide to Molecular Interactions. *J. Med. Chem. 53*, 5061–5084.
(24) Braun-Sand, S. O., Mats, H. M., and Warshel, A. (2005) Computer Modeling of Enzyme Catalysis and its Relationship to Concepts in Physical Organic Chemistry. *Adv. Phys. Org. Chem. 40*, 201–245.
(25) Lu, Y., Wang, Y., and Zhu, W. (2010) Nonbonding interactions of organic halogens in biological systems: Implications for drug discovery and biomolecular design. *Phys. Chem. Chem. Phys. 12*, 4543–4551.
(26) Chamberlain, B. T., Upton, T. G., Kashemirov, B. A., and McKenna, C. E. (2011) α-Azido bisphosphonates: Synthesis and nucleotide analogues. *J. Org. Chem. 76*, 5132–5136.
(27) Chamberlain, B. T., Batra, V. K., Beard, W. A., Kadina, A. P., Shock, D. D., Kashemirov, B. A., McKenna, C. E., Goodman, M. F., and Wilson, S. H. (2012) Stereospecific Formation of a Ternary Complex of (S)-α,β-Fluoromethylene-dATP with DNA Pol β. *ChemBioChem 13*, 528–530.
(28) Bakhtina, M., Roettger, M. P., and Tsai, M. D. (2009) Contribution of the reverse rate of the conformational step to polymerase β fidelity. *Biochemistry 48*, 3197–3208.
(29) Lin, P., Batra, V. K., Pedersen, L. C., Beard, W. A., Wilson, S. H., and Pedersen, L. G. (2008) Incorrect nucleotide insertion at the active site of a G:A mismatch catalyzed by DNA polymerase β. *Proc. Natl. Acad. Sci. U.S.A. 105*, 5670–5674.
(30) Lin, P., Pedersen, L. C., Batra, V. K., Beard, W. A., Wilson, S. H., and Pedersen, L. G. (2006) Energy analysis of chemistry for correct insertion by DNA polymerase β. *Proc. Natl. Acad. Sci. U.S.A. 103*, 13294–13299.
(31) Tsai, Y. C., and Johnson, K. A. (2006) A new paradigm for DNA polymerase specificity. *Biochemistry 45*, 9675–9687.
(32) Dalvit, C., and Vulpetti, A. (2011) Fluorine-protein interactions and ^{19}F NMR isotropic chemical shifts: An empirical correlation with implications for drug design. *ChemMedChem 6*, 104–114.
(33) Liu, D., Moran, S., and Kool, E. T. (1997) Bi-stranded, multisite replication of a base pair between difluorotoluene and adenine: Confirmation by 'inverse' sequencing. *Chem. Biol. 4*, 919–926.
(34) Lu, Y., Wang, Y., Xu, Z., Yan, X., Luo, X., Jiang, H., and Zhu, W. (2009) C-X···H contacts in biomolecular systems: How they contribute to protein-ligand binding affinity. *J. Phys. Chem. B 113*, 12615–12621.
(35) Moran, S., Ren, R. X., Rumney, S., and Kool, E. T. (1997) Difluorotoluene, a Nonpolar Isostere for Thymine, Codes Specifically and Efficiently for Adenine in DNA Replication. *J. Am. Chem. Soc. 119*, 2056–2057.
(36) Dalvit, C., and Vulpetti, A. (2012) Intermolecular and Intramolecular Hydrogen Bonds Involving Fluorine Atoms: Implications for Recognition, Selectivity, and Chemical Properties. *ChemMedChem 7*, 262–272.
(37) Wallwork, S. C. (1962) Hydrogen-Bond Radii. *Acta Crystallogr. 15*, 758–759.
(38) Aaqvist, J., and Warshel, A. (1993) Simulation of enzyme reactions using valence bond force fields and other hybrid quantum/classical approaches. *Chem. Rev. 93*, 2523–2544.